Calorimetric Study of Mixed Phosphates $Na_4M_3(PO_4)_2P_2O_7$ (M = Mn^{2+}, Fe^{2+}, Co^{2+}, Ni^{2+}) to Evaluate the Electrochemical Trends

K. Jayanthi, Shubham Lochab, Prabeer Barpanda, and Alexandra Navrotsky*

ABSTRACT: Mixed polyanionic compounds have been studied extensively as viable cathode materials for sodium-ion batteries. Mixed phosphates, $Na_4M_3(PO_4)_2P_2O_7$ (M = Mn^{2+}, Fe^{2+}, Co^{2+}, Ni^{2+}), provide a low barrier for Na-ion diffusion, b eing advantageous in comparison to phosphates and pyrophosphates. The reported order of sodium extraction is ambiguous and remains unclear. Despite being structurally similar, electrochemical performance differs f or a ll f our a nalogues w ith d ifferent degrees of (de)sodiation, according to the transition element present. Here, high-temperature oxide melt solution calorimetry has been used to establish the relation between thermodynamic phase stability and observed capacity for this series of mixed phosphates. Thermodynamic phase stability largely depends on the kind of structure, type of bonding, and size of the cations present. So, according to our results, the thermodynamic phase stability follows the order $Na_4Mn_3(PO_4)_2P_2O_7$ > $Na_4Fe_3(PO_4)_2P_2O_7$ > $Na_4Co_3(PO_4)_2P_2O_7$ > $Na_4Ni_3(PO_4)_2P_2O_7$. The thermodynamic studies serve as guidelines for the selection of compositions with the potential for fabricating advanced cathode materials with maximum performance.

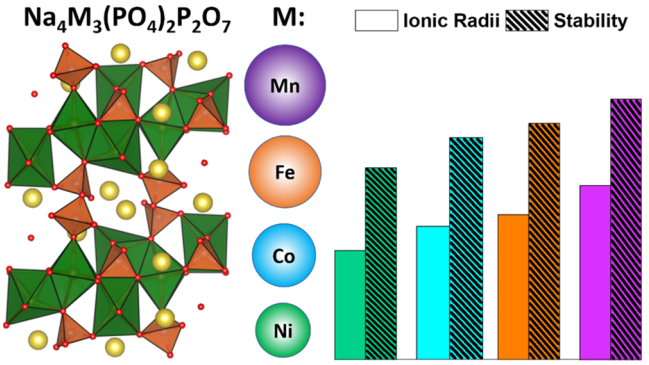

INTRODUCTION

Mixed phosphates with a general formula of $Na_4M_3(PO_4)_2P_2O_7$ (M = Mn^{2+}, Fe^{2+}, Co^{2+}, Ni^{2+}) are a promising class of polyanionic materials that can be used as cathodes for Na-ion batteries (NIBs). They have garnered attention because of the presence of low migration barriers and are advantageous as compared to simpler phosphates or pyrophosphates.[1−3] They provide three-dimensional diffusion, high operating voltage, and small volume change during electrochemical cycling with the persistence of the structure. In the Fe analogue, Fe^{+2}/Fe^{+3} redox leads to a higher value of voltage (3.1 V) than for $NaFePO_4$, $Na_2FeP_2O_7$, and Na_2FePO_4F.[4−6] The higher operating voltage is attributed to the inductive effect via the constituent phosphate and pyrophosphate groups. With the presence of more polyanionic units, a greater number of resonating structures are possible, which weakens the M−O covalent bond. So, there is a shorter distance between bonding and antibonding orbitals, which leads to a slightly higher voltage.[7] The redox potential can also be altered by changing the transition metal. Replacing Fe^{2+} with Mn^{2+}, Co^{2+}, or Ni^{2+} increases the redox potential. The iron analogue $Na_4Fe_3(PO_4)_2P_2O_7$ also shows less volume change during Na-ion (de)insertion (<4%) than $NaFePO_4$ (17%).[8] Degradation by moisture attack is also not observed in these mixed phosphates.[9]

Theoretically, if all four sodium ions are exchanged in $Na_4M_3(PO_4)_2P_2O_7$, the capacity obtained will be higher than that of sodium metal phosphates, $NaMPO_4$.[10−12] According to first-principles calculations, it is possible to exchange all four Na^+ ions in the cobalt analogue $Na_4Co_3(PO_4)_2P_2O_7$, where during the last sodium deinsertion, electron transfer happens from the oxygen sublattice instead of by Co^{+3}/Co^{+4} oxidation.[13] However, there is a narrowing of the channel during the last sodium-ion deinsertion. Large volume changes accompany the deinsertion at around 4.83 V, where the stability of the electrolyte also becomes an issue.[6] The theoretical capacity of $Na_4Co_3(PO_4)_2P_2O_7$ is calculated to be ~170 mAh/g, considering possible four Na^+-ion deinsertion. For the iron analogue $Na_4Fe_3(PO_4)_2P_2O_7$, theoretical capacity (129 mAh/g) is calculated based on three sodium-ion deinsertion, which is due to the narrowing of Na tunnels after the third Na-ion extraction and the improbable oxidation of Fe^{+2} to Fe^{+4}. Similar theoretical capacity calculations based on three sodium-ion (de)insertion have been reported for Mn and Ni analogues as well.[6,14]

Mixed phosphates, $Na_4M_3(PO_4)_2P_2O_7$ (M = Mn^{2+}, Fe^{2+}, Co^{2+}, Ni^{2+}), are isostructural with an orthorhombic $Pn2_1a$ space group with slight changes in cell volume (Mn > Fe > Co > Ni) (Table 1).[1,3,6] It consists of $[M_3P_2O_{13}]_n$ alternate double layers with corner-sharing and edge-sharing PO_4 tetrahedra and MO_6 octahedra, present parallel to the *bc* plane. The double layers are connected along the *a*-axis by pyrophosphate (P_2O_7) groups, which act as pillars to provide structural stability. A tunnel network is formed due to this linkage along the three crystallographic directions ([*100*], [*010*], [*001*]) containing Na cations. The transition metal occupies three distinct sites, and sodium ions are in four different crystallographic sites connected by three different channels (A, B and C) along the three axes (Figure 1i). Na(1) and Na(2) have a curved pathway, while Na(3) and Na(4) have a linear pathway.[2,14] The coordination number for Na ranges from 5 to 7, with the Na ion with a lower coordination number extracted first. This leads to a steep discharge profile and multiple redox peaks in the electrochemical curves (Figure 1k,l). The discharge potential for $Na_4M_3(PO_4)_2P_2O_7$ (M = Mn^{2+}, Fe^{2+}, Co^{2+}, Ni^{2+}) with an M^{+2}/M^{+3} redox activity is in the order Ni > Co > Mn > Fe due to different *d*-orbital splittings.[7] Based on the constituent transition metal present in the $Na_4M_3(PO_4)_2P_2O_7$ family, average redox potential values for sodium intercalation are Ni (4.8 V), Co (4.5 V), Mn (3.8 V), and Fe (3.1 V).[6]

Table 1. Space Group, Unit Cell Volume, Ionic Radius (M^{2+}), and Discharge Capacity

Sample	Ionic radius (pm)	Space group	Unit cell volume (Å^3)	Discharge capacity (mAh/g)
$Na_4Mn_3(PO_4)_2P_2O_7$	83	$Pn2_1a$	1286.80	121[23]
$Na_4Fe_3(PO_4)_2P_2O_7$	78	$Pn2_1a$	1260.53	121[29]
$Na_4Co_3(PO_4)_2P_2O_7$	74.5	$Pn2_1a$	1236.73	95[11]
$Na_4Ni_3(PO_4)_2P_2O_7$	69	$Pn2_1a$	1194.30	51[30]

Previous calorimetric studies from our group have provided insights into thermodynamic influence on the structure–property relationships in suites of battery materials. The observed energetics and electrochemical behavior were attributed to their structure, the difference in their ionic radii, and the corresponding effect on bonding, acid–base interactions, enhanced stability owing to hydration, and polymorphic phase selection.[15−22] In this paper, we have employed high-temperature oxide melt solution calorimetry to measure enthalpies of formation to elucidate the observed electrochemical behavior in the $Na_4M_3(PO_4)_2P_2O_7$ family. We found a strong correlation between the energetic stability and

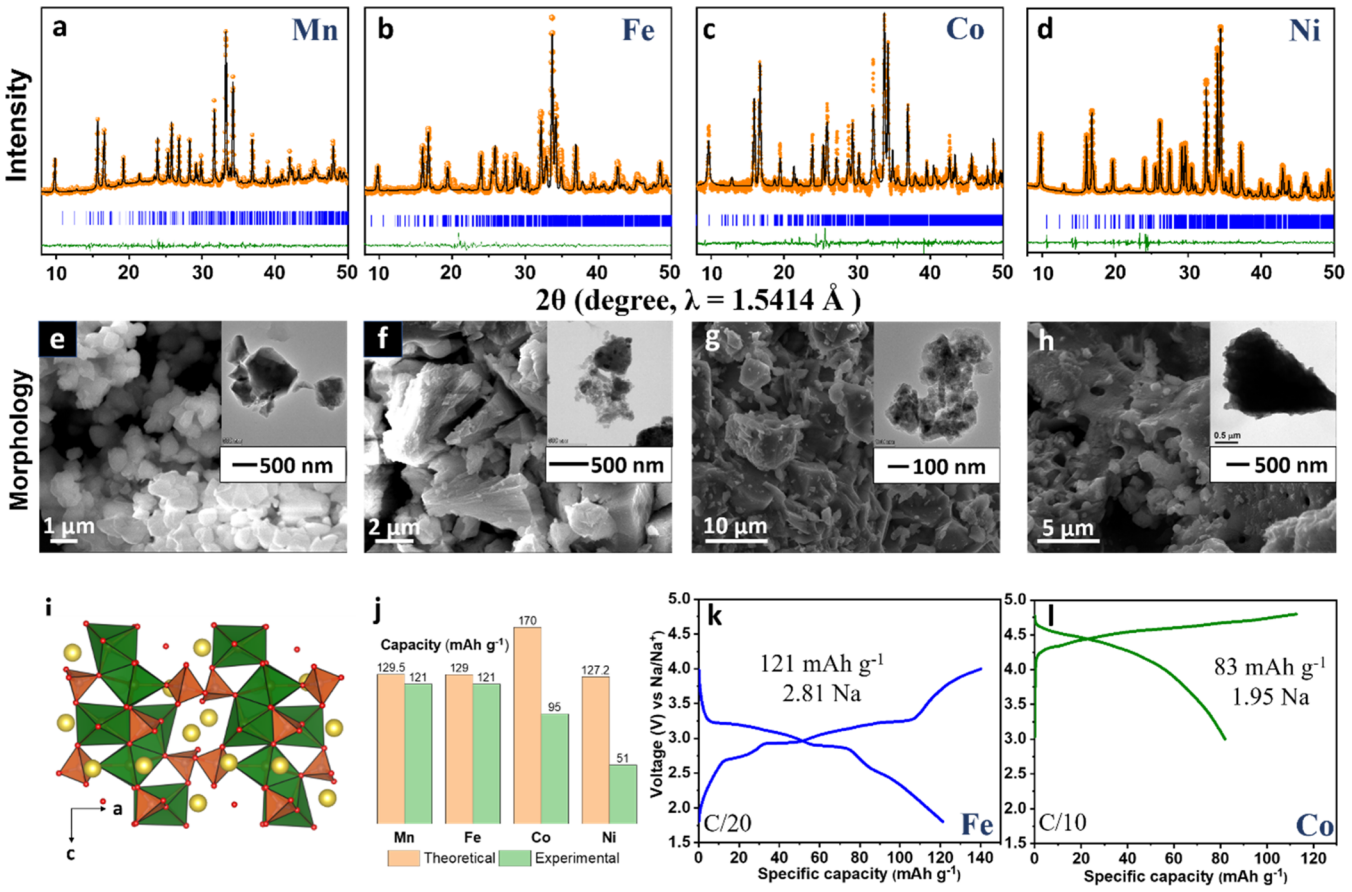

Figure 1. (a–d) Rietveld refinement of XRD patterns of $Na_4M_3(PO_4)_2P_2O_7$ (M = Mn^{2+}, Fe^{2+}, Co^{2+}, Ni^{2+}) made by solution combustion synthesis. Experimental data points (orange), calculated pattern (black), their difference (olive green), and Bragg reflections (blue ticks) are shown. (e–h) SEM images of the mixed phosphate analogues indicating porous particles, their size, and agglomeration. The inset shows the TEM images of the nanometric particles (100–500 nm scale). (i) Structural illustration of $Na_4M_3(PO_4)_2P_2O_7$ with pyrophosphate linkages. MO_6 octahedra (green), PO_4/P_2O_7 tetrahedra (orange), oxygen (red), and sodium (yellow) atoms are shown. (j) Comparison of theoretical and experimental capacity. (k, l) Representative galvanostatic (dis)charge voltage profiles for $Na_4M_3(PO_4)_2P_2O_7$ (M = Fe^{2+}, Co^{2+}).

ionic radii of the transition metal (M = Mn^{2+}, Fe^{2+}, Co^{2+}, Ni^{2+}), which provides insights into the observed trend in capacity.

EXPERIMENTAL METHODS

Synthesis and Characterization. $Na_4M_3(PO_4)_2P_2O_7$ (M = Fe^{2+}, Co^{2+}, Ni^{2+}) materials were prepared by solution combustion synthesis (SCS) using different precursors. Stoichiometric proportions (1:1) of sodium dihydrogen phosphate ($NaH_2PO_4{\cdot}H_2O$) and different nitrate precursors for each analogue along with ascorbic acid were dissolved in distilled water with thorough mixing to make a homogenous solution. Ascorbic acid acted as fuel as well as a reducing agent. The precursor solution was heated at 120 °C to evaporate excess water, and the temperature was then increased to 300 °C to start the exothermic combustion reaction. Gradual release of gases was observed, leading to a porous amorphous intermediate product that was ground, pressed into pellets, and calcined in a tubular furnace at 600 °C for 5 h (for Co, Ni analogues) and 600 °C for 12 h (for Fe analogue) under steady Ar flow to get the final products. For $Na_4Mn_3(PO_4)_2P_2O_7$, a conventional solid-state reaction was followed.[23] Stoichiometric amounts of $MnC_2O_4{\cdot}2H_2O$, $Na_4P_2O_7$, and $NH_4H_2PO_4$ were mixed together by wet ball-milling in acetone media at 400 rpm for 12 h. The slurry was dried at 70 °C for 12 h, and the resulting mixture was calcined at 300 °C for 6 h in air. The as-obtained intermediate powder was pelletized and calcined at 600 °C for 6 h (in air) to yield the final product.

For the as-synthesized mixed polyanionic materials, powder X-ray diffraction (XRD) patterns were collected with a PANalytical X'Pert Pro diffractometer with a Cu Kα target of a monochromatic wavelength of λ =1.5404 Å operating at 40 kV/30 mA. Diffractograms were acquired in the 2θ range 10−50° with a scanning step of 0.0268°/s in Bragg−Brentano geometry. Rietveld analysis was performed using the FullProf program, and the structures were illustrated using VESTA software.[24,25] The morphology of the mixed phosphate samples was characterized by combining a Carl Zeiss ULTRA55 FESEM scanning electron microscope (SEM) operating at 5 kV and an FEI Tecnai F20 S-Twin transmission electron microscope (TEM) operating at 200 kV.

Electrochemical Cell Testing. The pristine mixed phosphate powder was mixed with Super-P conducting carbon black and poly(vinylidene fluoride) (PVDF) binder in a ratio of 8:1:1 to form the working electrode. The composition was mixed thoroughly with *N*-methyl 2-pyrrolidone (NMP) to form a thick slurry, which was coated on an aluminum foil and dried at 80 °C under a vacuum. Prototype CR2032 type coin cells were assembled in an Ar-filled glovebox (MBraun LabStar GmbH, Germany) using the working electrode (cathode) and a sodium metal foil (anode) separated by a sheet of Whatman GF/C glass fiber separator soaked with a 1 M $NaPF_6$/ethylene carbonate (EC)/diethyl carbonate (DEC) (1:1 (v/v)) (Kishida Chemicals, Japan) electrolyte. The electrochemical activity of these half-cells was tested using a Neware BTS 4000 (Shenzhen, China) battery tester (at 25 °C).

High-Temperature Oxide Melt Solution Calorimetry. High-temperature oxide melt solution calorimetry was done using a Setaram AlexSYS Tian-Calvet twin microcalorimeter using methods standard to our laboratory and described in previous reports.[26−28] This calorimeter allows the direct determination of the enthalpy of formation ($\Delta H^\circ_{f,ox}$) of multicomponent compounds from the binary oxides. In a typical experiment, ∼5 mg of a $Na_4M_3(PO_4)_2P_2O_7$ sample was pelletized and dropped from ambient temperature into the calorimeter at 800 °C containing the solvent molten sodium molybdate ($3Na_2O{\cdot}4MoO_3$) in a platinum crucible. The measured enthalpy of drop solution (ΔH_{ds}) is a sum of the sample heat content from the ambient temperature to 800 °C and its heat of solution in the solvent at 800 °C. At least 8−10 experiments were done per sample, and the results are reported as average values with errors reported as two standard deviations of the mean. The calorimetry glassware was flushed by oxygen gas at a flow rate of 65 mL/min to maintain a constant atmosphere, and the solvent was bubbled with the same gas at 5 mL/min to remove liberated evolved gases, aid dissolution, and prevent local saturation of the solvent. The calorimeter was calibrated using the heat content of 5 mg pellets of α-Al_2O_3 (99.997%). The details of the calorimeter and procedures have been described previously.[17,20]

RESULTS AND DISCUSSION

Structure and Electrochemical Performance. The combustion-synthesized $Na_4M_3(PO_4)_2P_2O_7$ (M = Mn^{2+}, Fe^{2+}, Co^{2+}, Ni^{2+}) powders were confirmed to be phase pure from Rietveld refinement (Figure 1a−d and Tables S1−S4). The powders were well crystallized with particle size in the nanometric range with porous agglomerates formed in the micrometric range (Figure 1e−h). The production of nanoscale particles can be attributed to the solution combustion synthesis (SCS) method. This method generates a substantial amount of gaseous byproducts, causing a significant expansion of the solid product and a rapid decrease in temperature after the reaction is complete. These characteristics result in a final product that is porous, finely dispersed, and nanometric. The crystal structure for the mixed phosphate family is orthorhombic with space group $Pn2_1a$ (Table 1). Edge- and corner-shared MO_6 octahedra and PO_4 tetrahedra form $[M_3P_2O_{13}]_n$ double layers parallel to the *bc* plane. The layers are interconnected by P_2O_7 (pyrophosphate groups) along the *a*-direction. A three-dimensional tunnel network is formed along three crystallographic directions [*100*], [*010*], and [*001*], where sodium ions can also be hosted.

Within the mixed phosphate family, varied discharge capacities according to the transition metal present have been reported. Different values are attributed based on three or four Na-ion (de)insertion. Some reports suggest the extraction of the fourth sodium ion from $Na_4Co_3(PO_4)_2P_2O_7$ (NCPP) occurring at a high voltage of 4.8 V (vs Na), which would give a theoretical capacity value of 170 mAh/g. Possible reasons for this could be the Co^{+3}/Co^{+4} transition or oxidation of the lattice oxygen.[13] For $Na_4Fe_3(PO_4)_2P_2O_7$ (NFPP), Kim et al. highlighted the importance of the fourth sodium ion in the stability of the orthorhombic structure. Extraction of three sodium ions was found to be possible, indicating the theoretical capacity value to be 129 mAh/g.[10] In accordance with this analysis, most reports use three sodium-ion (de)insertion to calculate the theoretical capacity for $Na_4Mn_3(PO_4)_2P_2O_7$ (NMPP) and $Na_4Ni_3(PO_4)_2P_2O_7$ (NNPP) as well.

Figure 1j shows theoretical capacity values for the mixed phosphate family along with obtained experimental values. The observed capacity for the mixed phosphates is in the order NMPP (121 mAh/g, 2.8 Na^+) = NFPP (121 mAh/g, 2.8 Na^+) > NCPP (95 mAh/g, 2.2 Na^+) > NNPP (51 mAh/g, 1.3 Na^+) (Table 1). Figure S1 shows the cycling stability for

Table 2. Thermodynamic Cycles Used to Calculate Formation Enthalpies ($\Delta H°_{f,ox}$) of $Na_4M_3(PO_4)_2P_2O_7$ (M = Mn^{2+}, Fe^{2+}, Co^{2+}, Ni^{2+}) at 25 °C from the Oxides[a]

Reaction	ΔH
Cycle 1 (M = Co^{2+}, and Ni^{2+})	
$Na_4M_3(PO_4)_2P_2O_{7\ (s,\ 25\ °C)} \rightarrow 2Na_2O_{\ (sln,\ 800°C)} + 3MO_{\ (sln,\ 800°C)} + 2P_2O_{5\ (sln,\ 800°C)}$	ΔH_1
$Na_2O_{\ (s,\ 25\ °C)} \rightarrow Na_2O_{\ (sln,\ 800°C)}$	ΔH_2
$MO_{\ (s,\ 25\ °C)} \rightarrow MO_{\ (sln,\ 800°C)}$	ΔH_3
$P_2O_{5\ (s,\ 25\ °C)} \rightarrow P_2O_{5\ (sln,\ 800°C)}$	ΔH_4
$2Na_2O_{\ (s,\ 25\ °C)} + 3MO_{\ (s,\ 25\ °C)} + 2P_2O_{5\ (s,\ 25\ °C)} \rightarrow Na_4M_3(PO_4)_2P_2O_{7\ (s,\ 25\ °C)}$	$\Delta H°_{f,ox}$
$\Delta H°_{f,ox} = -\Delta H_1 + 2\Delta H_2 + 3\Delta H_3 + 2\Delta H_4$	
Cycle 2 (M = Fe^{2+})	
$Na_4Fe_3(PO_4)_2P_2O_{7\ (s,\ 25\ °C)} + 0.75O_{2\ (g,\ 25\ °C)} \rightarrow 2Na_2O_{\ (sln,\ 800°C)} + 1.5Fe_2O_{3\ (sln,\ 800°C)} + 2P_2O_{5\ (sln,\ 800°C)}$	ΔH_5
$Na_2O_{\ (s,\ 25\ °C)} \rightarrow Na_2O_{\ (sln,\ 800°C)}$	ΔH_6
$FeO_{\ (s,\ 25\ °C)} + 0.25O_{2\ (g,\ 25\ °C)} \rightarrow 0.5Fe_2O_{3\ (sln,\ 800°C)}$	ΔH_7
$P_2O_{5\ (s,\ 25\ °C)} \rightarrow P_2O_{5\ (sln,\ 800°C)}$	ΔH_8
$2Na_2O_{\ (s,\ 25\ °C)} + 3FeO_{\ (s,\ 25\ °C)} + 2P_2O_{5\ (s,\ 25\ °C)} \rightarrow Na_4Fe_3(PO_4)_2P_2O_{7\ (s,\ 25\ °C)}$	$\Delta H°_{f,ox}$
$\Delta H°_{f,ox} = -\Delta H_5 + 2\Delta H_6 + 3\Delta H_7 + 2\Delta H_8$	
Cycle 3 (M = Mn^{2+})	
$Na_4Mn_3(PO_4)_2P_2O_{7\ (s,\ 25\ °C)} + 0.75O_{2\ (g,\ 25\ °C)} \rightarrow 2Na_2O_{\ (sln,\ 800°C)} + 1.5Mn_2O_{3\ (sln,\ 800°C)} + 2P_2O_{5\ (sln,\ 800°C)}$	ΔH_9
$Na_2O_{\ (s,\ 25\ °C)} \rightarrow Na_2O_{\ (sln,\ 800°C)}$	ΔH_{10}
$MnO_{\ (s,\ 25\ °C)} + 0.25O_{2\ (g,\ 25\ °C)} \rightarrow 0.5Mn_2O_{3\ (s,\ 25°C)}$	ΔH_{11}
$Mn_2O_{3\ (s,\ 25\ °C)} \rightarrow Mn_2O_{3\ (sln,\ 800°C)}$	ΔH_{12}
$P_2O_{5\ (s,\ 25\ °C)} \rightarrow P_2O_{5\ (sln,\ 800°C)}$	ΔH_{13}
$2Na_2O_{\ (s,\ 25\ °C)} + 3MnO_{\ (s,\ 25\ °C)} + 0.75O_{2\ (g,\ 25\ °C)} + 2P_2O_{5\ (s,\ 25\ °C)} \rightarrow Na_4Fe_3(PO_4)_2P_2O_{7\ (s,\ 25\ °C)}$	$\Delta H°_{f,ox}$
$\Delta H°_{f,ox} = -\Delta H_9 + 2\Delta H_{10} + 3\Delta H_{11} + 1.5\Delta H_{12} + 2\Delta H_{13}$	

[a] $\Delta H_{11} = \Delta H_{rxn} = [0.5\Delta H°_{f,el}\ (Mn_2O_{3(s)}) - \Delta H°_{f,el}\ (MnO_{(s)})] = -94.30 \pm 0.71$ kJ/mol. s = solid; g = gas; sln = solution.

Table 3. Drop Solution Enthalpies (ΔH_{ds}) in $3Na_2O{\cdot}4MoO_3$ at 800 °C and Calculated Formation Enthalpies from Oxides ($\Delta H°_{f,ox}$) at 25 °C of $Na_4M_3(PO_4)_2P_2O_7$ (M = Mn^{2+}, Fe^{2+}, Co^{2+}, Ni^{2+}) Samples[a]

Sample	ΔH_{ds} (kJ/mol)	$\Delta H°_{f,ox}$ (kJ/mol)	$\Delta H°_{f,el}$ (kJ/mol)
$Na_4Mn_3(PO_4)_2P_2O_7$	775.10 ± 0.64	−1494.25 ± 8.78	
$Na_4Fe_3(PO_4)_2P_2O_7$	524.89 ± 0.75	−1466.18 ± 8.75	
$Na_4Co_3(PO_4)_2P_2O_7$	698.32 ± 0.91	−1332.35 ± 8.68	
$Na_4Ni_3(PO_4)_2P_2O_7$	666.94 ± 0.99	−1230.47 ± 8.80	
Na_2O	−195.90 ± 4.23[31]		
Mn_2O_3	175.69 ± 0.48 (7)		−959.00 ± 1.00[34]
MnO			−385.20 ± 0.50[34]
FeO	−80.50 ± 0.54 (6)		
CoO	21.92 ± 0.36 (8)[32]		
NiO	45.42 ± 0.58 (7)		
P_2O_5	−153.99 ± 0.68 (15)[33]		

[a] Value is the mean of the number of experiments indicated in parentheses. Two standard deviations are given as errors.

$Na_4Fe_3(PO_4)_2P_2O_7$ and $Na_4Co_3(PO_4)_2P_2O_7$ materials at a cycling rate of C/10. $Na_4Mn_3(PO_4)_2P_2O_7$ delivers a discharge capacity of 121 mAh/g at C/20 with an average redox potential of ∼3.84 V. $Na_4Fe_3(PO_4)_2P_2O_7$ exhibits a discharge capacity of 121 mAh/g with an average redox potential of 3.1 V. The full capacity value is considered unachievable in the case of $Na_4Co_3(PO_4)_2P_2O_7$ because of the activity of $Co^{+3/+4}$ at 4.8 V (vs Na). $Na_4Ni_3(PO_4)_2P_2O_7$ delivers the lowest experimental capacity of all four due to lower ionic conductivity and collapse of $[Ni_3P_2O_{13}]_n$ layers leading to sodium irreversibility. Due to a significant narrowing of the channels with each sodium-ion extraction from the $Na_4Ni_3(PO_4)_2P_2O_7$ material, major volume changes occur in the structure upon desodiation as sodium atoms act as pillars holding the $[Ni_3P_2O_{13}]_n$ layers together. This can lead to the collapse of these layers, accompanied by significant capacity loss with each subsequent cycle.[6] The ionic conductivity values of the $Na_4M_3(PO_4)_2P_2O_7$ family have been reported to exhibit significant differences. At a temperature of 330 °C, the ionic conductivity (σ_{300}) for $Na_4Mn_3(PO_4)_2P_2O_7$, $Na_4Co_3(PO_4)_2P_2O_7$, and $Na_4Ni_3(PO_4)_2P_2O_7$ is ∼10^{-5}, 10^{-6}, and 10^{-7} S/cm, respectively.[1] To better understand the different values of capacity obtained for the four analogues and the possibility of different degrees of (de)sodiation, we have investigated the thermodynamic stability of this mixed phosphate family.

Thermodynamic Studies. Thermal analysis (TG-DSC) measurements were performed before the calorimetric measurements to detect adsorbed water on the sample due to exposure in the ambient atmosphere prior to calorimetric experiments. There was no mass loss confirming the absence of any adsorbed water on the samples.

The enthalpies of formation ($\Delta H°_{f,ox}$) from Na_2O, the corresponding transition metal oxide, MO (M = Mn^{2+}, Fe^{2+}, Co^{2+}, Ni^{2+}), and P_2O_5 were calculated at 25 °C using the thermochemical cycle in Table 2. The enthalpies of the drop solution (ΔH_{ds}) for series of $Na_4M_3(PO_4)_2P_2O_7$, FeO, and NiO were measured, and values for Na_2O, CoO, Mn_2O_3, and

P_2O_5 are taken from previously published work.[31−33] Enthalpy of the drop solution of MnO is calculated using the enthalpy of formation from elements[34] for the oxidation reaction of MnO to Mn_2O_3 in order to maintain uniformity in assessing the enthalpy of the formation values obtained for Fe, Co, and Ni.

The measured ΔH_{ds} values for $Na_4M_3(PO_4)_2P_2O_7$ are endothermic, ranging from 524.89 ± 0.75 to 775.10 ± 0.64 kJ/mol. The calculated $\Delta H^\circ_{f,ox}$ values are −1494.25 ± 8.78, −1466.18 ± 8.75, −1332.35 ± 8.68, and −1230.47 ± 8.80 kJ/mol, for $Na_4Mn_3(PO_4)_2P_2O_7$, $Na_4Fe_3(PO_4)_2P_2O_7$, $Na_4Co_3(PO_4)_2P_2O_7$, and $Na_4Ni_3(PO_4)_2P_2O_7$, respectively. $\Delta H^\circ_{f,ox}$ values are highly exothermic, confirming the thermodynamic stability in $Na_4M_3(PO_4)_2P_2O_7$ series. Table 3 and Figure 2a show the correlation of formation enthalpies

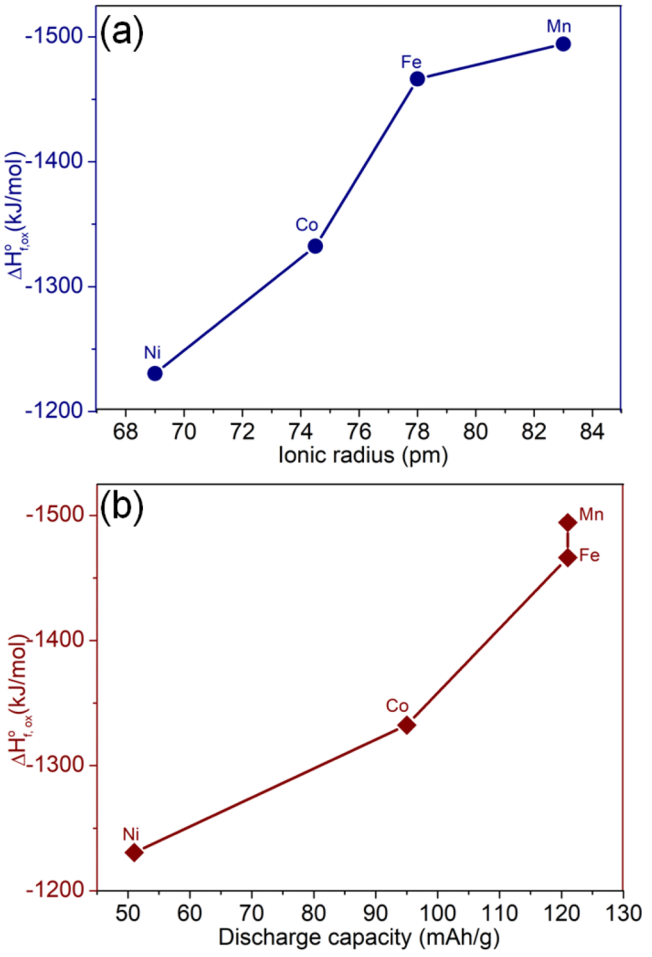

Figure 2. Enthalpy of formation as a function of (a) ionic radius and (b) discharge capacity for $Na_4M_3(PO_4)_2P_2O_7$ (M = Mn^{2+}, Fe^{2+}, Co^{2+}, Ni^{2+}) series.

with the ionic radius; $\Delta H^\circ_{f,ox}$ becomes less exothermic with a decrease in the ionic radius of the M^{2+}, attributing to stronger M−O interaction (Figure 2a). A similar trend has been observed in $\Delta H^\circ_{f,ox}$ for $NaMO_2$[16] and both monoclinic and orthorhombic $Li_2M(SO_4)_2$ except for Ni.[35]

Figure 2b shows formation enthalpy as a function of discharge capacity. $Na_4Mn_3(PO_4)_2P_2O_7$ is most energetically stable with $\Delta H^\circ_{f,ox}$ = −1494.25 ± 8.78 kJ/mol with the highest discharge capacity (121 mAh/g), while $Na_4Ni_3(PO_4)_2P_2O_7$ is least stable with $\Delta H^\circ_{f,ox}$ = −1230.47 ± 8.80 with the lowest discharge capacity (51 mAh/g). The discharge capacity varies linearly with the energetic stability of these materials. Kim et al. attribute the high power capability and cycle stability of a manganese-based cathode in sodium-ion cells to the unique Jahn−Teller distortion in this material.[23] Furthermore, they show that the sodium-ion mobility in this structure is not diminished by the structural changes induced by Jahn−Teller distortion (Mn^{3+}) as seen in most other manganese-based electrodes. In contrast, mobility is enhanced due to the distortion, which opens the sodium diffusion channels, as shown by DFT calculations.[23] A three-dimensional network for sodium-ion diffusion is observed without an increase in the activation barrier for Na hopping post distortion. Since ionic mobility depends directly on the diffusion pathways, enhanced ionic mobility is observed. This feature favors high cycle stability and high-power performance for sodium rechargeable batteries.[23] The enhanced sodium-ion mobility allows rapid sodium (de)insertion at various stages of charge of the electrode. The material also shows the largest Mn^{+2}/Mn^{+3} redox potential, i.e., 3.84 V, reported till now for manganese-based cathodes, as well as the highest energy density of 416 Wh/kg. The high voltage is due to the strong electron-withdrawing pyrophosphate P_2O_7 groups with a greater inductive effect present around the Mn octahedra. Also, in the desodiated structure, there is a Mn^{+3}−Mn^{+3} repulsion that leads to destabilization of the charged stage and increases the voltage obtained.[23] Because of the high voltage and large energy density with good cycling stability, $Na_4Mn_3(PO_4)_2P_2O_7$ can be employed as a cathode material for Na-ion batteries.

CONCLUSIONS

$Na_4M_3(PO_4)_2(P_2O_7)$ have gained attention as potential sodium battery cathodes owing to the fast diffusion of Na ions with a low migration barrier and enhanced performance compared to individual phosphate and pyrophosphate compounds. The $Na_4M_3(PO_4)_2(P_2O_7)$ (M = Mn^{2+}, Fe^{2+}, Co^{2+}, Ni^{2+}) series exhibits highly exothermic enthalpies of formation. There is a strong correlation between the thermodynamic stability and the ionic radius of the transition metal. The stable $Na_4Mn_3(PO_4)_2(P_2O_7)$ delivers higher discharge capacity compared to least stable $Na_4Ni_3(PO_4)_2(P_2O_7)$. Thermodynamic stability relative to binary oxides diminishes in the order $Na_4Mn_3(PO_4)_2P_2O_7$ > $Na_4Fe_3(PO_4)_2P_2O_7$ > $Na_4Co_3(PO_4)_2P_2O_7$ > $Na_4Ni_3(PO_4)_2P_2O_7$. The high voltage, large energy density, cycle stability, and the use of low-cost Mn give $Na_4Mn_3(PO_4)_2(P_2O_7)$ significant potential as a promising cathode material for large-scale Na-ion batteries.

AUTHOR INFORMATION

Corresponding Author

Alexandra Navrotsky − *School of Molecular Sciences and Navrotsky Eyring Center for Materials of the Universe,*

Arizona State University, Tempe, Arizona 85287, United States; orcid.org/0000-0002-3260-0364;
Email: Alexandra.Navrotsky@asu.edu

Authors

K. Jayanthi − *School of Molecular Sciences and Navrotsky Eyring Center for Materials of the Universe, Arizona State University, Tempe, Arizona 85287, United States; Chemical Sciences Division, Oak Ridge National Laboratory, Oak Ridge, Tennessee 37831, United States;* orcid.org/0000-0002-5016-3575

Shubham Lochab − *Faraday Materials Laboratory (FaMaL), Materials Research Centre, Indian Institute of Science, Bangalore 560012, India*

Prabeer Barpanda − *Faraday Materials Laboratory (FaMaL), Materials Research Centre, Indian Institute of Science, Bangalore 560012, India; Electrochemical Energy Storage, Helmholtz Institute Ulm (HIU), Ulm 89081, Germany; Institute of Nanotechnology, Karlsruhe Institute of Technology (KIT), Karlsruhe 76021, Germany;* orcid.org/0000-0003-0902-3690

Notes

The authors declare no competing financial interest.

ACKNOWLEDGMENTS

K.J. and A.N. acknowledge the U.S. Department of Energy Office of Basic Energy Sciences, Grant DE-SC0021987, for calorimetric measurements and thermodynamic analysis. The current work was partially supported by the Technology Mission Division (DST, Government of India) under the Materials for Energy Storage (MES-2018) program (DST/TMD/MES/2k18/00217). S.L. thanks Dr. S.P. Adiga for hosting him at Samsung R&D Centre Bangalore during the project work. S.L. is grateful to the Ministry of Human Resource Development (MHRD, Government of India) for financial support. P.B. is grateful to Alexander von Humboldt Foundation (Bonn, Germany) for a 2022 Humboldt fellowship for experienced researchers.

REFERENCES

(1) Sanz, F.; Parada, C.; Rojo, J. M.; Ruíz-Valero, C. Synthesis, Structural Characterization, Magnetic Properties, and Ionic Conductivity of $Na_4M_3^{II}(PO_4)_2(P_2O_7)$ (M^{II} = Mn, Co, Ni). *Chem. Mater.* **2001**, *13*, 1334−1340.

(2) Kim, H.; Park, I.; Seo, D.-H.; Lee, S.; Kim, S.-W.; Kwon, W. J.; Park, Y.-U.; Kim, C. S.; Jeon, S.; Kang, K. New Iron-Based Mixed-Polyanion Cathodes for Lithium and Sodium Rechargeable Batteries: Combined First Principles Calculations and Experimental Study. *J. Am. Chem. Soc.* **2012**, *134*, 10369−10372.

(3) Sanz, F.; Parada, C.; Amador, U.; Monge, M. A.; Valero, C. R. $Na_4Co_3(PO_4)_2P_2O_7$, a New Sodium Cobalt Phosphate Containing a Three-Dimensional System of Large Intersecting Tunnels. *J. Solid State Chem.* **1996**, *123*, 129−139.

(4) Niu, Y.; Zhang, Y.; Xu, M. A Review on Pyrophosphate Framework Cathode Materials for Sodium-Ion Batteries. *J. Mater. Chem. A* **2019**, *7*, 15006−15025.

(5) Senthilkumar, B.; Murugesan, C.; Sharma, L.; Lochab, S.; Barpanda, P. An Overview of Mixed Polyanionic Cathode Materials for Sodium-Ion Batteries. *Small Methods* **2019**, *3*, No. 1800253.

(6) Gezović, A.; Vujković, M. J.; Milović, M.; Grudić, V.; Dominko, R.; Mentus, S. Recent Developments of $Na_4M_3(PO_4)_2(P_2O_7)$ as the Cathode Material for Alkaline-Ion Rechargeable Batteries: Challenges and Outlook. *Energy Storage Mater.* **2021**, *37*, 243−273.

(7) Gutierrez, A.; Benedek, N. A.; Manthiram, A. Crystal-Chemical Guide for Understanding Redox Energy Variations of $M^{2+/3+}$ Couples in Polyanion Cathodes for Lithium-Ion Batteries. *Chem. Mater.* **2013**, *25*, 4010−4016.

(8) Casas-Cabanas, M.; Roddatis, V. V.; Saurel, D.; Kubiak, P.; Carretero-González, J.; Palomares, V.; Serras, P.; Rojo, T. Crystal Chemistry of Na Insertion/Deinsertion in $FePO_4$−$NaFePO_4$. *J. Mater. Chem.* **2012**, *22*, 17421−17423.

(9) Kosova, N. V.; Rezepova, D. O.; Podgornova, O. A.; Slobodyuk, A. B.; Petrov, S. A.; Avdeev, M. A Comparative Study of Structure, Air Sensitivity and Electrochemistry of Sodium Iron Pyrophosphates $Na_{2-x}Fe_{1+x/2}P_2O_7$ (x = 0; 0.44). *Electrochim. Acta* **2017**, *235*, 42−55.

(10) Kim, S.-W.; Seo, D.-H.; Ma, X.; Ceder, G.; Kang, K. Electrode Materials for Rechargeable Sodium-Ion Batteries: Potential Alternatives to Current Lithium-Ion Batteries. *Adv. Energy Mater.* **2012**, *2*, 710−721.

(11) Nose, M.; Nakayama, H.; Nobuhara, K.; Yamaguchi, H.; Nakanishi, S.; Iba, H. $Na_4Co_3(PO_4)_2P_2O_7$: A Novel Storage Material for Sodium-Ion Batteries. *J. Power Sources* **2013**, *234*, 175−179.

(12) Nose, M.; Shiotani, S.; Nakayama, H.; Nobuhara, K.; Nakanishi, S.; Iba, H. $Na_4Co_{2.4}Mn_{0.3}Ni_{0.3}(PO_4)_2P_2O_7$: High Potential and High Capacity Electrode Material for Sodium-Ion Batteries. *Electrochem. Commun.* **2013**, *34*, 266−269.

(13) Moriwake, H.; Kuwabara, A.; Fisher, C. A. J.; Nose, M.; Nakayama, H.; Nakanishi, S.; Iba, H.; Ikuhara, Y. Crystal and Electronic Structure Changes During the Charge-Discharge Process of $Na_4Co_3(PO_4)_2P_2O_7$. *J. Power Sources* **2016**, *326*, 220−225.

(14) Wood, S. M.; Eames, C.; Kendrick, E.; Islam, M. S. Sodium Ion Diffusion and Voltage Trends in Phosphates $Na_4M_3(PO_4)_2P_2O_7$ (M = Fe, Mn, Co, Ni) for Possible High-Rate Cathodes. *J. Phys. Chem. C* **2015**, *119*, 15935−15941.

(15) Singh, S.; Jha, P. K.; Avdeev, M.; Zhang, W. L.; Jayanthi, K.; Navrotsky, A.; Alshareef, H. N.; Barpanda, P. Marinite $Li_2Ni(SO_4)_2$ as a New Member of Bisulfate Family of High-Voltage Lithium Battery Cathodes. *Chem. Mater.* **2021**, *33*, 6108−6119.

(16) Radha, A. V.; Lander, L.; Rousse, G.; Tarascon, J. M.; Navrotsky, A. Thermodynamic Stability and Correlation with Synthesis Conditions, Structure and Phase Transformations in Orthorhombic and Monoclinic $Li_2M(SO_4)_2$ (M = Mn, Fe, Co, Ni) Polymorphs. *J. Mater. Chem. A* **2015**, *3*, 2601−2608.

(17) Jayanthi, K.; Chaupatnaik, A.; Barpanda, P.; Navrotsky, A. Probing Capacity Trends in $MLi_2Ti_6O_{14}$ Lithium-Ion Battery Anodes Using Calorimetric Studies. *ACS Omega* **2022**, *7*, 42482−42488.

(18) Barman, P.; Dwibedi, D.; Jayanthi, K.; Meena, S. S.; Nagendra, S.; Navrotsky, A.; Barpanda, P. Aqueous Spray-Drying Synthesis of Alluaudite $Na_{2+2x}Fe_{2-x}(SO_4)_3$ Sodium Insertion Material: Studies of Electrochemical Activity, Thermodynamic Stability and Humidity Induced Phase Transition. *J. Solid State Electrochem.* **2022**, *26*, 1941−1950.

(19) Radha, A. V.; Subban, C. V.; Sun, M. L.; Tarascon, J. M.; Navrotsky, A. Possible Correlation Between Enthalpies of Formation and Redox Potentials in $LiMSO_4OH$ (M = Co, Fe, Mn) Li-ion

Polyanionic Battery Cathode Materials. *J. Mater. Chem. A* **2014**, *2*, 6887−6894.
(20) Barman, P.; Jha, P. K.; Chaupatnaik, A.; Jayanthi, K.; Prasada Rao, R.; Sai Gautam, G.; Franger, S.; Navrotsky, A.; Barpanda, P. A New High Voltage Alluaudite Sodium Battery Insertion Material. *Mater. Today Chem.* **2023**, *27*, No. 101316.
(21) Singh, S.; Neveu, A.; Jayanthi, K.; Das, T.; Chakraborty, S.; Navrotsky, A.; Pralong, V.; Barpanda, P. Facile Synthesis and Phase Stability of Cu-based $Na_2Cu(SO_4)_2.xH_2O$ (x = 0-2) Sulfate Minerals as Conversion Type Battery Electrodes. *Dalton Trans.* **2022**, *51*, 11169−11179.
(22) Radha, A. V.; Furman, J. D.; Ati, M.; Melot, B. C.; Tarascon, J. M.; Navrotsky, A. Understanding the Stability of Fluorosulfate Li-ion Battery Cathode Materials: A Thermochemical Study of $LiFe_{1-x}Mn_xSO_4F$ ($0 \leq x \leq 1$) Polymorphs. *J. Mater. Chem.* **2012**, *22*, 24446−24452.
(23) Kim, H.; Yoon, G.; Park, I.; Park, K.-Y.; Lee, B.; Kim, J.; Park, Y.-U.; Jung, S.-K.; Lim, H.-D.; Ahn, D.; et al. Anomalous Jahn−Teller Behavior in a Manganese-Based Mixed-Phosphate Cathode for Sodium Ion Batteries. *Energy Environ. Sci.* **2015**, *8*, 3325−3335.
(24) Rodríguez-Carvajal, J. *An Introduction to the Program FullProf 2000*; Laboratoire Léon Brillouin: Saclay, France; 2001.
(25) Momma, K.; Izumi, F. VESTA 3 for Three-Dimensional Visualization of Crystal, Volumetric and Morphology Data. *J. Appl. Crystallogr.* **2011**, *44*, 1272−1276.
(26) Navrotsky, A. Progress and New Directions in High Temperature Calorimetry. *Phys. Chem. Miner.* **1977**, *2*, 89−104.
(27) Navrotsky, A. Progress and New Directions in High Temperature Calorimetry Revisited. *Phys. Chem. Miner.* **1997**, *24*, 222−241.
(28) Navrotsky, A. Progress and New Directions in Calorimetry: A 2014 Perspective. *J. Am. Chem. Soc.* **2014**, *97*, 3349−3359.
(29) Senthilkumar, B.; Murugesan, C.; Sada, K.; Barpanda, P. Electrochemical Insertion of Potassium Ions in $Na_4Fe_3(PO_4)_2P_2O_7$ mixed phosphate. *J. Power Sources* **2020**, *480*, No. 228794.
(30) Kumar, P. R.; Yahia, H. B.; Belharouak, I.; Sougrati, M. T.; Passerini, S.; Amin, R.; Essehli, R. Electrochemical Investigations of High-Voltage $Na_4Ni_3(PO_4)_2P_2O_7$ Cathode for Sodium-Ion Batteries. *J. Solid State Electrochem.* **2020**, *24*, 17−24.
(31) Yang, S.; Anderko, A.; Riman, R. E.; Navrotsky, A. Thermochemistry of Sodium Rare Earth Ternary Fluorides, $NaREF_4$. *Acta Mater.* **2021**, *220*, No. 117289.
(32) Hayun, S.; Lilova, K.; Salhov, S.; Navrotsky, A. Enthalpies of Formation of High Entropy and Multicomponent Alloys Using Oxide Melt Solution Calorimetry. *Intermetallics* **2020**, *125*, No. 106897.
(33) Gibson, L. D.; Jayanthi, K.; Yang, S.; Thiele, N.; Anovitz, L. M.; Sacci, R. L.; Navrotsky, A.; Bryantsev, V. S. Characterization of Lanthanum Monazite Surface Chemistry and Crystal Morphology through Density Functional Theory and Experimental Approaches. *J Phys. Chem. C* **2022**, *126*, 18952−18962.
(34) Robie, R. A.; Hemingway, B. S. *Thermodynamic Properties of Minerals and Related Substances at 298.15 K and 1 Bar (105 Pascals) Pressure and at Higher Temperatures*; US Government Printing Office, 1995; Vol. *213*.
(35) Shivaramaiah, R.; Tallapragada, S.; Nagabhushana, G. P.; Navrotsky, A. Synthesis and Thermodynamics of Transition Metal Oxide Based Sodium Ion Cathode Materials. *J. Solid State Chem.* **2019**, *280*, No. 121011.